Chromate Reduction and Retention Processes within Arid Subsurface Environments

ARTICLE *in* ENVIRONMENTAL SCIENCE AND TECHNOLOGY · OCTOBER 2005

Impact Factor: 5.33 · DOI: 10.1021/es050535y · Source: PubMed

5 AUTHORS, INCLUDING:

Matthew Ginder-Vogel
University of Wisconsin–Madison
47 PUBLICATIONS **1,786** CITATIONS
SEE PROFILE

Thomas Borch
Colorado State University
72 PUBLICATIONS **1,295** CITATIONS
SEE PROFILE

Melanie Mayes
Oak Ridge National Laboratory
72 PUBLICATIONS **683** CITATIONS
SEE PROFILE

Scott Fendorf
Stanford University
270 PUBLICATIONS **10,823** CITATIONS
SEE PROFILE

Environ. Sci. Technol. **2005**, *39,* 7833−7839

Chromate Reduction and Retention Processes within Arid Subsurface Environments

MATTHEW GINDER-VOGEL,[†] THOMAS BORCH,[†,§] MELANIE A. MAYES,[‡] PHILLIP M. JARDINE,[‡] AND SCOTT FENDORF*,[†]

Department of Geological and Environmental Sciences, Stanford University, Stanford, California 94305, and Oak Ridge National Laboratory, Oak Ridge, Tennessee 37831

Chromate is a widespread contaminant that has deleterious impacts on human health, the mobility and toxicity of which are diminished by reduction to Cr(III). While biological and chemical reduction reactions of Cr(VI) are well resolved, reduction within natural sediments, particularly of arid environments, remains poorly described. Here, we examine chromate reduction within arid sediments from the Hanford, WA site, where Fe(III) (hydr)oxide and carbonate coatings limit mineral reactivity. Chromium(VI) reduction by Hanford sediments is negligible unless pretreated with acid; acidic pretreatment of packed mineral beds having a Cr(VI) feed solution results in Cr(III) associating with the minerals antigorite and lizardite in addition to magnetite and Fe(II)-bearing clay minerals. Highly alkaline conditions (pH > 14), representative of conditions near high-level nuclear waste tanks, result in Fe(II) dissolution and concurrent Cr(VI) reduction. Additionally, Cr(III) and Cr(VI) are found associated with portlandite, suggesting a secondary mechanism for chromium retention at high pH. Thus, mineral reactivity is limited within this arid environment and appreciable reduction of Cr(VI) is restricted to highly alkaline conditions resulting near leaking radioactive waste disposal tanks.

Introduction

Chromium enters the environment primarily through its widespread use in industrial applications, including tanning, metallurgy, and plating. Once introduced, it persists as either Cr(VI) or Cr(III). Hexavalent Cr exists in groundwater systems as the oxyanion $H_xCrO_4^{x-2}$ (chromate), which exhibits high water solubility and is a mutagen, teratogen, and carcinogen (*1*). In contrast, Cr(III) is relatively nontoxic and strongly partitions to the solid phase (*2*).

Chromium(VI) can be reduced to Cr(III) by aqueous and sorbed Fe(II) (*3*, *4*), organic matter (*5*), Fe(II)-bearing minerals (*6*−*8*), sulfide compounds (*9*, *10*), and through microbial processes (*11*). These reductants all ultimately lead to Cr(III), but the rates and products differ. Enzymatic reduction of chromate may result in the formation of soluble organic Cr(III) complexes (*12*−*14*), while chromate reduction by soluble Fe(II) results in the formation of $Cr_{1-x}Fe_x(OH)_3$ precipitates (*2*).

Subsurface chromate contamination is a major environmental threat at the U.S. Department of Energy's Hanford Site (southeastern Washington State, USA), the location of plutonium production starting during World War II. The climate of the Hanford Site is arid, with an average rainfall of 15.9 cm y^{-1}, resulting in a 10−60 m deep vadose zone (*16*). In the 100 Area of the Hanford Site, chromate used as a corrosion inhibitor in nuclear reactor cooling water was discharged to unlined surface cribs, resulting in chromate contamination reaching the Columbia River (*16*), which is not only a primary source of drinking water, but also a spawning-ground for salmon. Additionally, thousands of liters of hot (100 °C), caustic (pH > 14), chromate-containing high-level nuclear waste (HLW) from the reduction−oxidation (REDOX) plutonium recovery process has leaked into the vadose zone, as a result of multiple failures of single-shell tanks in the S-SX tank farm (*17*). Should chromate from these tanks reach the water table, rapid migration to the Columbia River would result. Analysis of chromium's redox state in a core obtained from a HLW plume beneath tank SX 108 revealed that 29−75% of the total Cr had been reduced to Cr(III) (*18*).

In aerobic, arid environments, with limited organic carbon (such as the Hanford Site), chromate reductants are essentially restricted to Fe(II)-bearing mineral phases of geologic origin. The uppermost principal geologic unit of the Hanford Site consists of material deposited in cataclysmic ice age floods during the past 12 000−700 000 y, termed the Hanford formation. Potential sources of Fe(II) in the Hanford sediments include iron-bearing silicates such as lizardite [$Mg_xFe_{3-x}Si_2O_5(OH)_4$] (this work), antigorite [$(Mg,Fe)_3Si_2O_5(OH)_4$] (this work), biotite (*19*), magnetite, and ilmenite (*19*). Chromate reduction by Fe(II)-bearing minerals is controlled by their surface reactivity. Mineral surface coatings such as carbonates (*20*), silicates, and Fe(III) (hydr)oxides (*6*, *15*) inhibit electron transfer from underlying Fe(II) to aqueous Cr(VI), all of which commonly form in the vadose zone of arid environments.

In the Hanford subsurface, chromium contamination has occurred in two distinct geochemical environments, termed the "near-field" and "far-field" environments in this Article. The near-field environment is adjacent to leaking tanks of HLW and is characterized by high pH, salt concentration, and temperature, resulting in extensive mineral dissolution and surface modification. The far-field environment is representative of the background geochemical conditions (circumneutral pH, ambient temperature, etc.). These conditions are relevant at locations far from a leaking tank and in arid environments in general.

Chromate reduction by Fe(II) (aq), magnetite, ilmenite, and biotite has been studied extensively in model systems at acidic and neutral pH (*6*, *9*, *21*, *22*), and in the case of magnetite (*23*) and Fe(II) (aq) (*24*), at high pH as well. What remains elusive are the minerals serving as chromate reductants and the factors limiting (or promoting) chromate reduction within arid soils and sediments. In the present work, we examine the reduction of chromate by sediment obtained from the Hanford formation beneath the Interim Disposal Facility (IDF) at the Hanford Site. The objectives of this study are to determine what geochemical conditions are required for chromate reduction by Hanford formation sediments and which minerals are a source of chromate reduction. In addition to providing information about chromate reduction specific to the Hanford Site, these

* Corresponding author phone: (650)723-5238; fax: (650)723-2199; e-mail: fendorf@stanford.edu.
† Stanford University.
‡ Oak Ridge National Laboratory.
§ Present address: Department of Soil and Crop Sciences, Colorado State University, Fort Collins, CO 80523.

10.1021/es050535y CCC: $30.25
Published on Web 09/17/2005

TABLE 1. Experimental Conditions Used in Columns To Investigate Chromate Reduction by Hanford Formation Sediment[a]

column ID	pretreatment	influent solution	influent pH	Cr retained (mmol Cr g^{-1} sediment)
control	none	0.2 mM $CaCl_2$, 0.2 mM K_2CrO_4	8	1.0×10^{-5}
10 M NaOH	none	10 M NaOH, 0.2 mM K_2CrO_4	>14	1.1×10^{-3}
sonicated	8 h sonication	0.2 mM $CaCl_2$, 0.2 mM K_2CrO_4	8	1.0×10^{-5}
10 mM oxalate	10 PV[b] 10 mM oxalate	0.2 mM $CaCl_2$, 0.2 mM K_2CrO_4	8	1.1×10^{-5}
acid-treated	10 PV 0.5 M HCl	0.2 mM $CaCl_2$, 0.2 mM K_2CrO_4	8	8.3×10^{-4}
base-treated	10 PV 0.5 M NaOH	0.2 mM $CaCl_2$, 0.2 mM K_2CrO_4	8	9.1×10^{-6}
0.2 mM Cr(VI)	10 PV 0.5 M HCl	0.2 mM $CaCl_2$, 0.2 mM K_2CrO_4	8	7.0×10^{-4}
0.1 mM Cr(VI)	10 PV 0.5 M HCl	0.2 mM $CaCl_2$, 0.1 mM K_2CrO_4	8	1.0×10^{-3}
0.02 mM Cr(VI)	10 PV 0.5 M HCl	0.2 mM $CaCl_2$, 0.02 mM K_2CrO_4	8	8.7×10^{-4}

[a] After pretreatment, and prior to the introduction of the chromate influent solution, all columns were equilibrated with 10 pore volumes of 0.2 mM $CaCl_2$ at pH 8. [b] PV = pore volumes.

experiments provide generally applicable information about abiotic chromate reduction pathways in natural media, particularly relevant to soils and sediments of arid environments.

Materials and Methods

Sediment Description. Sediments were obtained from borehole C3177, drilled during 2001 in the 200 East Area, at the northeast corner of the Interim Disposal Facility (IDF) of the Hanford Site. A detailed description of the core collection and geochemistry is available in Horton et al. (*25*) and Walker et al. (*26*). Briefly, the <2 mm size fractions of five composite samples from depths of 14, 34, 46, 61, and 66 m below ground surface in the Hanford flood sediments were used in this study. These sediment samples are referred to as IDF-1−IDF-5, in order of increasing depth. Horton et al. (2003) reports pH values of 7.3, 7.4, 7.5, 7.5, and 7.6 for IDF-1−5, respectively, and that the total carbon content of each sediment is less than 2.6 g kg^{-1}. All samples are mineralogically similar to the sand-size fraction dominated by quartz, Na- and K-feldspars, and mica and the clay-size fraction dominated by smectite, chlorite, illite, and kaolinite (*25*). Hanford formation sediments contain trace amounts of magnetite, ilmenite, and biotite (*19*). The Fe content of the samples was 44, 49, 43, 61, and 77 g kg^{-1} for IDF-1−5, respectively, as determined by XRF (*25*).

Column Design and Reaction Conditions. Experiments were conducted to determine factors responsible for or limiting chromate reduction in the Hanford sediments (Table 1). The porosity of all packed columns was approximately 53%, with an average pore volume of 7.9 ± 0.1 cm^3. Flow velocities upward through columns were maintained at ca. 1.7 pore volumes per day. All columns except the 10 M NaOH were run at least until the concentration of Cr(VI) in the effluent was equal to the influent concentration (complete Cr(VI) breakthrough). To simulate arid environments, oxygen was not excluded from any of the column systems, and the influent solutions were adjusted to pH 8, approximating the pH of the sediments (*25*). At the conclusion of each experiment, breakthrough curves were obtained for 0.2 mM $CaBr_2$ (pH 8); the sediments were then removed and stored at 10 °C.

Chromate reduction under near-field conditions was investigated using two columns packed with 15 g of dry IDF-5 sediment. Columns were saturated with 0.2 mM $CaCl_2$ prior to the introduction of a control solution or the feed solution containing 0.2 mM K_2CrO_4 in 10 M NaOH.

The impact of mineral coatings was evaluated in a second set of experiments using various sediment pretreatments. Here, one column was packed with 15 g of IDF-4 sediment that had been sonicated in Milli-Q water for 8 h. Three additional columns were packed with 15 g of dry IDF-4 sediment and then pretreated with 10 pore volumes of 10 mM oxalate, 0.5 M HCl, or 0.5 M NaOH; a final, untreated column was used as a control. All five columns were then equilibrated with 10 pore volumes of 0.2 mM $CaCl_2$ at pH 8. Finally, flow of a solution of 0.2 mM K_2CrO_4 and 0.2 mM $CaCl_2$, adjusted to pH 8, was initiated.

A final series of experiments was conducted using three columns packed with 15 g of dry IDF-5 sediment. Three of these columns were treated with 10 pore volumes of 0.5 M HCl, while an untreated column was used as a control. The four columns were equilibrated with 10 pore volumes of 0.2 mM $CaCl_2$ at pH 8. Flow of a chromate-containing feed solution was then initiated. The feed solution for the control column contained 0.2 mM K_2CrO_4, while the feed solutions of the acid-treated columns contained either 0.2, 0.1, or 0.02 mM K_2CrO_4. All feed solutions also contained 0.2 mM $CaCl_2$ and were adjusted to pH 8 with 5 mM NaOH. Using a regression model, the 95% confidence interval of the uptake curves was established at ±0.2 mmol Cr Kg^{-1} sediment.

Solution and Solid-Phase Measurements. Effluent pH was determined with an Orion ROSS electrode. Total soluble Cr, Si, Al, Ca, and Fe were measured in samples passed through a 0.2 μm polymer filter using a Thermo Jarrell Ash IRIS inductively coupled plasma optical emission spectrometer. Iron(II) and chromium(VI) were analyzed colorimetrically by the ferrozine (*27*) and 1,5-diphenyl carbazide (*28*) methods, respectively. Solid-phase chromium concentrations were determined by extraction of 0.5 g of sediment with 2 mL of concentrated trace metal grade HNO_3 for 48 h. Bromide concentrations were determined using ion chromatography (Dionex, DX-500).

Solid-Phase Micro-Analysis. Synchrotron micro-X-ray fluorescence (μ-XRF) mapping and micro-X-ray absorption spectroscopy (μ-XAS) measurements were performed on beamline 10.3.2 at the Advanced Light Source (ALS, Berkeley, CA), GSE-CARS beamline 13-ID-C at the Advanced Photon Source (APS, Argonne, IL), and beamline X26A at the National Synchrotron Light Source (NSLS, Brookhaven, NY). Energy

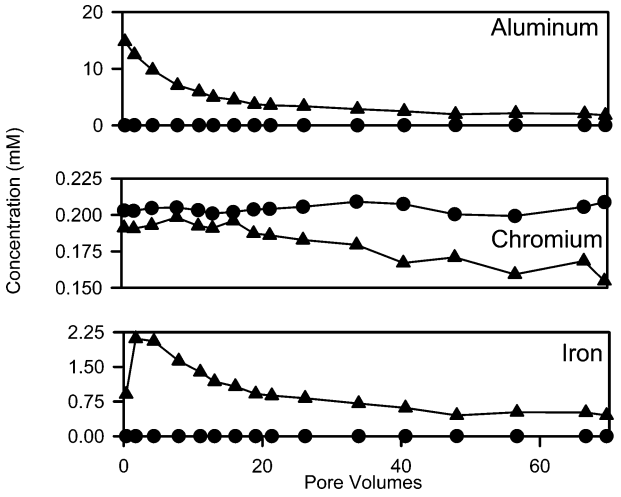

FIGURE 1. Effluent metal concentration for control (●) and 10 M NaOH columns (▲).

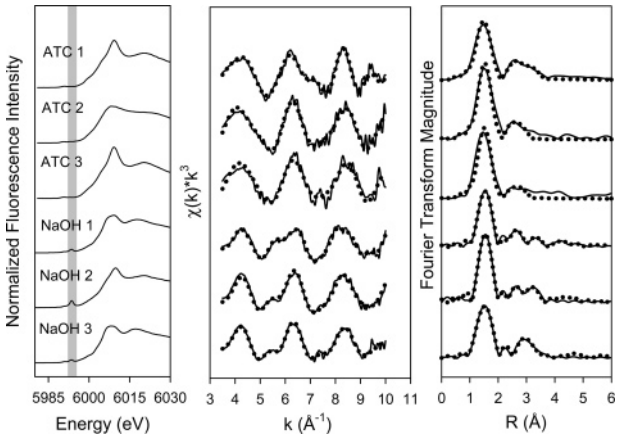

FIGURE 2. Chromium K-edge XANES (left), EXAFS (center), and Fourier transformed EXAFS (right) spectra from three areas of high Cr concentration in sediments from acid pretreated (ATC 1−3) and 10 M NaOH (NaOH 1−3) column experiments. EXAFS data (center; solid lines) were fit (center, dotted lines) over $k = 3.5-10$ Å^{-1} (fit data provided in Table 2). Fourier transforms of data (right, solid lines) and fits (right, dotted lines) were calculated over the same k range.

selection at the ALS and NSLS was accomplished with a water-cooled Si(111) monochromator and at the APS with a liquid N_2-cooled Si (111) monochromator. The incident X-ray beam was focused to a size of either 5 × 5 μm (ALS) or 5 × 10 μm (APS and NSLS), using two Si mirrors in a Kirkpatrick-Baez geometry. Sediments from the batch reactions were mounted on Kapton tape and X-ray fluorescence spectra were recorded on selected regions of the samples, on the basis of elemental associations obtained from μ-XRF maps.

XAS data were processed using the SixPACK interface to (*29*) IFEFFIT (*30*). XANES data were background-subtracted and normalized to a unit-edge step. After background subtraction and normalization, the EXAFS data were extracted and k^3-weighted. Phase and amplitude functions for shell-by-shell fitting were generated using FEFF 7 (*31*). A set of reference standards for Fe was utilized to perform linear combination k^3-weighted EXAFS spectral fitting, using SixPACK's least-squares fitting module, which is a graphical interface for IFEFFIT's minimization function (*30*). Linear combination fitting routines were used to reconstruct the experimental spectrum to determine the relative percentages of mineral phases. Shell-by-shell and linear combination fits were optimized by minimizing reduced χ^2 (*32*). The ratio of the Cr pre-edge peak to post-edge amplitude was used to determine the concentration of Cr(VI) (*10*).

Micro-XRD patterns were collected at ALS beamline 10.3.2 and NSLS beamline X26A on select areas in transmission geometry using monochromatic radiation (14, 16, or 17 keV) and a Bruker X-ray CCD camera. The resulting images were processed using FIT2D (*33*). The sample-to-detector distance and geometric corrections were calculated from the pattern of α-Al_2O_3. After these corrections were applied, the 2D images were integrated radially to yield 1D powder diffraction patterns that could then be analyzed using standard techniques. Peak identification and background correction, including removal of the scattering from the Kapton tape, were performed in JADE 6.5 (Materials Data, Inc., Livermore, CA).

Results

Impact of Alkaline Conditions on Cr(VI) Retention under Flow Conditions. To simulate mineral reactivity under near-field geochemical conditions (beneath a leaking tank), a feed solution of 10 M NaOH, containing 0.2 mM K_2CrO_4, was utilized. Chromate removal is observed in the first pore-volume of effluent. After 40 pore volumes, the effluent chromate concentration was 0.16 mM (Figure 1) and remained below the influent concentration (0.2 mM) until the termination of the experiment. The removal of Cr(VI) does not appear correlated with changes in aqueous Fe or Al concentration (Figure 1).

The Cr(VI) pre-edge feature (*10*, *21*) in XANES spectra reveals Cr(VI) in all identified Cr hot spots (Figure 2, NaOH 1−3), which is confirmed by the presence of Cr−O shells at 1.6 Å in the EXAFS spectra (Figure 2, Table 2). The points of high Cr concentration in the 10 M NaOH column contain 13−26% Cr(VI) and exhibit a Cr−Cr(Fe) structure similar to α/β-MeOOH (Me = Fe or Cr) (Figure 2, Table 2), with scattering contributions from Al(Si) at ∼3.1 Å, consistent with aluminum substitution, and Cr(Fe) at ∼3.5 Å. Comparatively, goethite (α-FeOOH) has Fe−Fe shells at 3.01, 3.29, and 3.43 Å (*34*) and akaganeite (β-FeOOH) at 3.03, 3.34, 3.50, and 3.55 Å (*35*). Lizardite and portlandite (CaOH) were commonly associated with high chromium concentrations (Figure 3A−D), and magnetite was detected in one sample (Figure 4C). A chromium-rich grain of portlandite was also isolated (Figures 3B, 4A), in which 20% of the chromium resides as Cr(VI) (data not shown).

Dissolution of Fe(II)-bearing minerals (antigorite, biotite, lizardite, and magnetite), induced by the extreme alkalinity, leads to the dispersal of Fe(II) and consequential chromate reduction/retention throughout the mineral matrix, as exemplified by a detailed examination of a hand-picked mica grain (Figure 4A). XANES spectra obtained from several points show Cr(III), and line scans across the particle indicate that Cr is distributed throughout the mineral surface (Figure 4A). Despite the preponderance of Cr(III), Cr(VI) was noted within the sample, in part through sequestration within portlandite (Figures 3B and 4A). As a result of the multiple retention mechanisms, 1.1 mmol Cr Kg^{-1} sediment is retained in the column reacted with a feed solution containing 10 M NaOH (Table 1).

Influence of Sediment Pretreatment on Chromate Retention under Flow Conditions. Chromate reduction by nontreated IDF-5 sediment was investigated under far-field conditions (those representative of the "native" geochemistry), using a feed solution of 0.2 mM K_2CrO_4 in 0.2 mM $CaCl_2$ adjusted to pH 8. Chromate breakthrough is commensurate with Br^-, indicating limited to no retardation (Figure 5). Several pretreatments were then used to target different types of surface coatings that may inhibit electron transfer from underlying Fe(II) to Cr(VI). Sonication was used to simulate physical abrasion, 0.5 M NaOH to promote

TABLE 2. Structural Parameters Derived from Least-Squares Fits to Raw k^3-Weighted Cr-EXAFS Spectra at Three Areas of High Cr Concentration in Sediments from Acid Pretreated (ATC 1−3) and 10 M NaOH (NaOH 1−3) Column Experiments[a]

	ATC 1			ATC 2			ATC 3			NaOH 1			NaOH 2			NaOH 3		
shell	r(Å)	CN	σ^2	r(Å)	CN	σ^2	r(Å)	CN	σ^2	r(Å)	CN	σ^2	r(Å)	CN	σ^2	r(Å)	CN	σ^2
Cr−O	NA	NA	NA	NA	NA	NA	NA	NA	NA	1.64(1)	2.9(2)	0.003(2)	1.66(9)	3.3(4)	0.015(4)	1.62(4)	2.9(3)	0.012(4)
Cr−O	1.98(1)	5.4(6)	0.002(2)	1.99(1)	5.8(4)	0.002(3)	1.99(1)	5.7(3)	0.003(2)	2.00(1)	4.8(2)	0.003(1)	1.99(1)	5.3(4)	0.003(5)	1.99(1)	5.0(3)	0.008(3)
Cr−Al(Si)	NA	NA	NA	NA	NA	NA	NA	NA	NA	3.08(1)	1.0(2)	0.002(3)	3.14(5)	0.8(3)	0.002(3)	NA	NA	NA
Cr−Cr(Fe)	3.18(8)	0.4(5)	0.002(1)	3.11(4)	1.9(9)	0.010(3)	3.19(1)	2.4(6)	0.004(3)	3.48(2)	2.1(3)	0.013(2)	3.45(5)	2.8(4)	0.010(4)	3.48(5)	2.8(4)	0.007(4)
Cr−Cr(Fe)	NA	NA	NA	NA	NA	NA	NA	NA	NA	4.68(4)	1.1(2)	0.003(1)	NA	NA	NA	3.64(8)	1.7(2)	0.007(3)
Cr−Cr(Fe)	NA	NA	NA	NA	NA	NA	NA	NA	NA	5.20(4)	0.5(2)	0.003(1)	NA	NA	NA	NA	NA	NA

[a] Coordination number (CN), interatomic distance (r), and Debye−Waller factor (σ^2) were obtained by fitting data with theoretical phase and amplitude functions. Fits were performed over a k range of 3.5−10 Å^{-1}. The reduced χ^2 values for each fit were between 0.6 and 0.9. Distances reported in the table differ from those in the radial distribution function (RDF) because the latter were not corrected for phase shift. Estimated errors at 95% confidence interval from the least-squares fit are given in parentheses.

dissolution of silicate phases, 10 mM oxalate to provide a complexant to dissolve Fe(III) and other metal (hydr)oxide phases, and 0.5 M HCl to induce acidic dissolution of metal oxide and carbonate phases. Ferrous iron was noted only in the acid treatment, with 160 mmol Fe(II) kg^{-1} removed, and this was the only system to retard Cr(VI) breakthrough (Figure 5); solid phase Cr was exclusively in the trivalent state (Figure 2). As a consequence of Cr reduction in the 0.5 M HCl-treated column, nearly 2 orders of magnitude more chromium is deposited than in unaltered solids (Table 1). The effluent pH of the 0.5 M HCl treated column was initially 6.5 and gradually increased to 7.5 over the duration of the experiment. The effluent pH of the other four columns was 7.7 ± 0.2 for the duration of the experiment.

Chromate retention within acid pretreated sediments was further examined at three influent chromate concentrations (0.2, 0.1, and 0.02 mM). Chromate breakthrough occurs after the elution of 20 pore volumes of 0.2 mM Cr(VI), 40 pore volumes of 0.1 mM Cr(VI), or 100 pore volumes of 0.02 mM Cr(VI) (S1). A comparison of the breakthrough trends, on a mass-introduced to mass-retained basis, reveals two distinct regions of Cr uptake by the sediment. An initial region occurs after introducing between 0 and 0.007 mmol of Cr(VI), and a second region occurs after introducing 0.007 mmol of Cr(VI) (S1). At the highest concentration (0.2 mM), retention is finite, while at 0.1 and 0.02 mM Cr(VI), continued Cr(VI) attenuation (tailing) results (S1; Table 1).

At all three influent concentrations, chromate reduction occurs concurrently with the presence of aqueous Fe(II) (S2). Prior to the introduction of Cr(VI), aqueous Fe(II) concentrations are below 0.002 mM (data not shown). Upon initiating the chromate-containing feed solution, aqueous Fe(II) levels increase and serve as a reductant of Cr(VI). Once the aqueous Fe(II) concentration decreases below 0.005 mM, chromate reduction ceases.

Reactive Solid Phases after Acid Treatment. High concentrations of reduced chromium associated with mafic minerals, including lizardite, antigorite (Figure 3E), and nimite, a ferrous iron-bearing phyllite (Figure 3F), were noted by μ-XRD. Chromium(III) was observed along the edges of mica grains (Figure 4B). Two iron μ-EXAFS spectra obtained from areas on XRF maps of high Cr concentrations are well fit by linear combinations of ferrihydrite-nontronite and ferrihydrite-biotite (S3).

EXAFS spectroscopy was used to probe the local structure of the mixed Cr/Fe (hydr)oxides precipitated at points of high Cr concentration in solid samples from the acid-treated column. Similar to the alkaline system, shell-by-shell fitting reveals mixed Cr/Fe precipitates in three spots of high-Cr concentration in the sediment from the acid-treated column (ATC) indicative of an α/β-MeOOH-like structure (Figure 2 and Table 2).

Discussion

During weathering in arid, oxic subsurface environments, Fe(II)-bearing mineral reactivity, with respect to chromate, becomes compromised by a variety of weathering rinds and surface coatings. Zachara et al. (*36*), for example, observed ferric (hydr)oxide rinds on biotite grains obtained from the Hanford formation sediments. In fact, using XPS analysis, we observe a ferric iron layer overlying magnetite separated from IDF 5 sediments (S4). The presence of such an oxidized layer diminishes the rate of chromate reduction due to limited transfer of electrons [or Fe(II)] from the underlying unoxidized mineral to the aqueous interface, as illustrated for synthetic magnetite (*6*). Because of the passivating layer on Fe(II)-bearing minerals, physical abrasion from fast shaking speeds is required for chromate reduction within batch reactions (S5), and acid or strong base treatment is needed for reduction within column experiments.

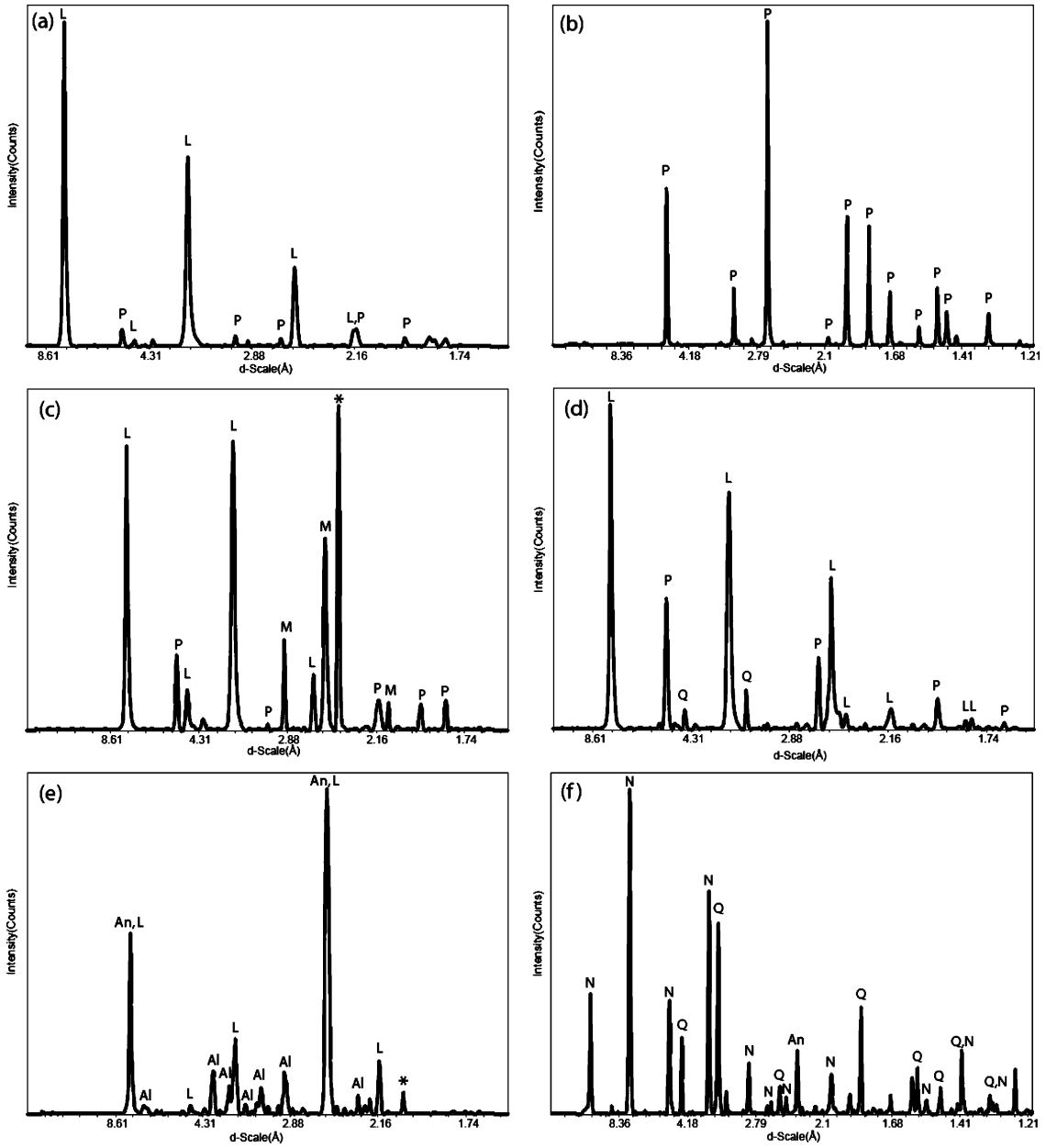

FIGURE 3. XRD patterns obtained from areas of high chromium concentration in sediments from 10 M NaOH (a−d) and acid pretreated (e,f) columns. Minerals identified in the patterns include portlandite (P), lizardite (L), magnetite (M), quartz (Q), nimite (N), antigorite (An), and albite (Al). Unidentifiable single scattering peaks are indicated with an "∗".

Under near-field tank conditions (10 M NaOH), the extreme pH induces base-catalyzed dissolution of both surface coatings (e.g., Fe-(hydr)oxides) and Fe(II)-bearing silicate minerals themselves. Under these conditions, columns having a 10 M NaOH feed solution retain more chromium than either acid pretreated or control columns (Table 1), and continue sequestering Cr at experiment termination (Figure 1) due to surface activation and extensive mineral dissolution. In this hyperalkaline system, XRF maps, combined with localized XRD analysis, reveal the association of high local chromium concentrations with several Fe(II)-bearing minerals, including antigorite, lizardite, and magnetite (Figure 3). EXAFS analysis of localized Cr(III) phases reveals that they have the short-range order consistent with an α/β MeOOH structure (Figure 2 and Table 2), suggesting that homogeneous Cr(VI) reduction by Fe(II) (aq) is occurring in addition to heterogeneous Cr(VI) reduction observed on mica grains (Figure 4).

The presence of portlandite is also detected in every instance of Cr deposition. Analysis of an isolated portlandite grain indicates Cr in association with the grain (Figures 3 and 4), 20% of which is in the hexavalent oxidation state. XANES analysis of three additional areas of high chromium concentration reveals Cr(VI) concentrations ranging from 13% to 26% (Figure 2). The presence of solid-phase Cr(VI) suggests that in addition to chromate reduction and subsequent precipitation, other retention mechanisms are partially responsible for the large amount of chromium retained under simulated near-field (i.e., hyperalkaline) conditions. Reduction of Cr(VI) to Cr(III) is likely inducing rapid nucleation and precipitation of portlandite, thereby trapping Cr(VI) in the solid phase. The retention of Cr(VI) at the Hanford Site has also been observed in sediment from a contaminated core obtained beneath tank SX-108, which contained Cr(VI) in addition to discrete Cr(III) mineral phases (*18*).

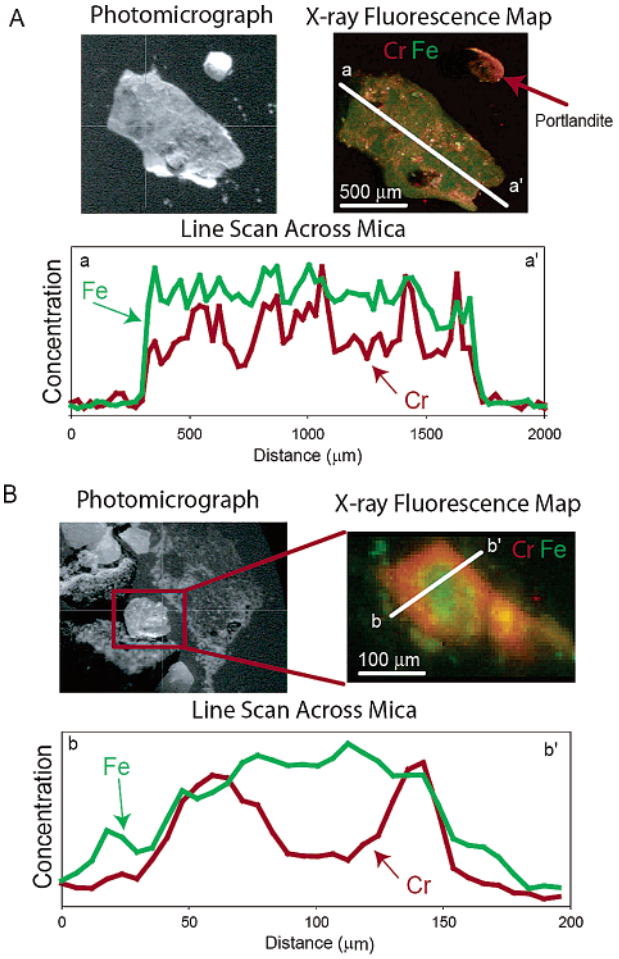

FIGURE 4. Microanalysis of mica grains from 10 M NaOH (A) and acid pretreated (B) columns. In XRF maps, Cr distribution is shown in red and Fe is shown in green.

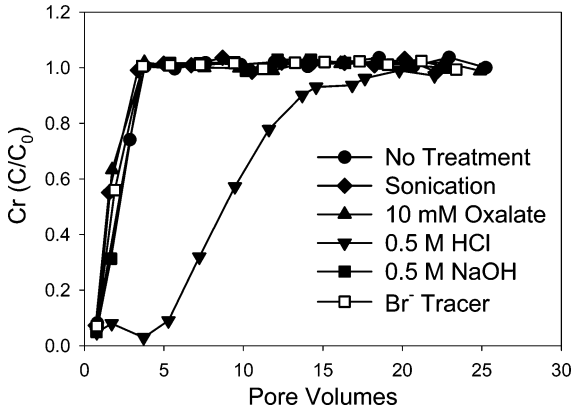

FIGURE 5. Effect of sediment pretreatment on Cr(VI) breakthrough. The sediment was pretreated with 10 pore volumes of the indicated treatment, followed by equilibration with 10 pore volumes of 0.2 mM $CaCl_2$ at pH 8, prior to the introduction of the 0.2 mM K_2CrO_4 solution.

The impact of oxidized surface coatings on Cr(VI) reduction by Fe(II)-bearing minerals is exemplified by the sediment pretreatment experiments, where chromate reduction is only observed after the acidic dissolution of Fe(III) (hydr)oxide surface coatings (Figure 5). Similar to the alkaline column, localized high-chromium concentrations are associated with Fe(II)-bearing minerals including biotite, antigorite, lizardite, and nimite (a ferrous-bearing phyllosilicate) (Figure 3 and S3); however, less chromium is retained by the sediment (Table 1). The relationship of dissolved Fe and Cr in column-effluent (S2) suggests that initial Cr(VI) reduction is being mediated by soluble Fe(II). Chromium(VI) concentrations are anticorrelated with Fe(II) concentrations, and Cr(VI) is not detected in the effluent until Fe(II) decreases below 0.005 mM. Acidic pretreatment results in the activation of a limited number of Fe(II) surface sites (Figure 4B), and, as chromate reduction proceeds, it becomes self-inhibited by the oxidation of the underlying mineral phase and precipitation of mixed Cr(III)/Fe(III) (hydr)oxide phases (Figure 2, ATC 1−3, and S3). A feed solution containing 0.2 mM Cr(VI) results in more rapid surface passivation than the lower influent chromate concentrations of 0.1 and 0.02 mM (S1). However, due to competition of Cr(VI) for Fe(II) with molecular oxygen in aerated systems, less chromate is reduced in the 0.02 mM column than the 0.1 mM column due, in part, to a 5-fold longer reaction period to achieve comparable Cr quantities (Table 1 and S1).

Implications. Attenuation of chromate in arid environments will be governed by the reactivity of Fe(II)-bearing mineral phases, which is controlled by mineral solubility and surface reactivity. Chromate reduction by sediments of the Hanford formation under native geochemical conditions (pH < 8) is inhibited by surface coatings and low mineral solubility. Acidic dissolution of Fe(III) (hydr)oxide layers restores the redox activity of Fe(II) minerals resulting in chromate reduction; however, generation of Cr(III) and Fe(III) (hydr)oxide surface layers during Cr(VI) reduction further comprises redox activity. Conversely, near-field conditions (pH > 14) cause extensive base-induced mineral dissolution and Fe(II) release, resulting in chromate retention throughout the mineral matrix.

Serpentine subgroup minerals (i.e., lizardite and antigorite) are quite common and widely distributed in mafic rocks (their quantification, unfortunately, is compromised by kaolin minerals (*37*)). Up to 60% of the total iron in lizardite occurs in the reduced state; likewise, 90% of the total iron in antigorite occurs in the reduced state (*38*, *39*). This accounts for 3% and 40% of the octahedrally coordinated cations in lizardite and antigorite, respectively. Therefore, the contributions of magnetite notwithstanding, they combine with biotite to comprise an important reservoir of Fe(II) for chromate reduction. Under conditions that induce silicate mineral dissolution, such as the near-field geochemical environment at the Hanford Site, chromate reduction will thus be enhanced by release of Fe(II). Therefore, to thoroughly evaluate chromate reduction in arid environments, viable reductants under the relevant geochemical conditions must be considered. Given the paucity of organic matter within such systems, primary Fe(II)-bearing mineral phases will likely be the dominant reductants. The surface reactivity and solubility of such minerals thus need to be appreciated in deciphering the rate and extent of chromate reduction.

Acknowledgments

We are grateful to Royce Sparks and Molly Pace for laboratory assistance with the batch experiments. We thank Matthew Marcus (ALS), Steve Sutton and Matt Newville (APS), and Tony Lanzirotti (NSLS) for their help in synchrotron-based data acquisition, Sam Webb for his help in data analysis, and Paul Bertsch for his generous help in acquiring beamtime at the NSLS. We also thank R. Jeffrey Serne of Pacific Northwest National Laboratory for providing the IDF sediments and Kathleen Beman for editorial input. This research was supported by the U.S. Department of Energy's EMSP Program (grant number DE-FG07-02ER63516). Portions of this work were performed at GeoSoilEnviroCARS (Sector 13), Advanced Photon Source (APS), Argonne National Laboratory. GeoSoilEnviroCARS is supported by the National Science Foundation-Earth Sciences (EAR-0217473), Department of Energy-

Geosciences (DE-FG02-94ER14466), and the State of Illinois. Use of the APS was supported by the U.S. Department of Energy, Basic Energy Sciences, Office of Energy Research, under Contract No. W-31-109-Eng-38. The Advanced Light Source is supported by the Director, Office of Science, Office of Basic Energy Sciences, Materials Sciences Division, of the U.S. Department of Energy under Contract No. DE-AC03-76SF00098 at Lawrence Berkeley National Laboratory. Research was also carried out at the National Synchrotron Light Source, Brookhaven National Laboratory, which is supported by the U.S. Department of Energy, Division of Materials Sciences and Division of Chemical Sciences, under Contract No. DE-AC02-98CH10886.

Supporting Information Available

Data pertaining to the effect of chromate concentration on breakthrough (S1, S2), Fe-EXAFS spectra obtained from areas of high Cr concentration (S3), XPS spectra of magnetic separates from IDF-5 (S4), and chromate uptake curves from batch experiments (S5). This material is available free of charge via the Internet at http://pubs.acs.org.

Literature Cited

(1) Fendorf, S. Surface reactions of chromium in soils and waters. *Geoderma* **1995**, *67*, 55−71.
(2) Sass, B. M.; Rai, D. Solubility of amorphous chromium(III)-iron(III) hydroxide solid solutions. *Inorg. Chem.* **1987**, *26*, 2228−2232.
(3) Fendorf, S.; Li, G. Kinetics of chromate reduction by ferrous iron. *Environ. Sci. Technol.* **1996**, *30*, 1614−1617.
(4) Buerge, I. J.; Hug, S. J. Influence of mineral surfaces on Cr(VI) reduction by iron(II). *Environ. Sci. Technol.* **1999**, *33*, 4285−4291.
(5) Deng, B.; Stone, A. T. Surface-catalyzed Cr(VI) reduction: Reactivity comparisons of different organic reductants and different oxide surfaces. *Environ. Sci. Technol.* **1996**, *30*, 2484−2494.
(6) Peterson, M. L.; White, A. F.; Brown, G. E.; Parks, G. A. Surface passivation of magnetite by reaction with aqueous Cr(VI): XAFS and TEM results. *Environ. Sci. Technol.* **1997**, *31*, 1573−1576.
(7) White, A. F.; Peterson, M. L. Reduction of aqueous transition metals on the surfaces of Fe(II)-containing oxides. *Geochim. Cosmochim. Acta* **1996**, *60*, 3799−3814.
(8) Bond, D. L.; Fendorf, S. Kinetics and structural constraints of chromate reduction by green rusts. *Environ. Sci. Technol.* **2003**, *27*, 2750−2757.
(9) Eary, L. E.; Rai, D. Kinetics of chromate reduction by ferrous ions derived from hematite and biotite at 25 °C. *Am. J. Sci.* **1989**, *289*, 180−213.
(10) Patterson, R. R.; Fendorf, S.; Fendorf, M. Reduction of hexavalent chromium by amorphous iron sulfides. *Environ. Sci. Technol.* **1997**, *31*, 2039−2044.
(11) Fendorf, S.; Wielinga, B. W.; Hansel, C. M. Chromium transformations in natural environments: The role of biological and abiological processes in chromium(VI) reduction. *Int. Geol. Rev.* **2000**, *42*, 691−701.
(12) James, B. J.; Bartlett, R. J. Behavior of chromium in soils: V. Fate of organically complexed Cr(III) added to soil. *J. Environ. Qual.* **1983**, *12*, 169−172.
(13) Puzon, G. J.; Peterson, J. N.; Roberts, A. G.; Kramer, D. M.; Xun, L. A bacterial flavin reductase system reduces chromate to a soluble chromium(III)-NAD+ complex. *Biochem. Biophys. Res. Commun.* **2002**, *294*, 76−81.
(14) Brauer, S. L.; Hneihen, A. S.; Wetterhahn, K. E. Chromium(VI) forms thiolate complexes with gamma-glutamylcysteine, N-acetcylcysteine, cysteine, and the methyl ester of n-acetylcysteine. *Inorg. Chem.* **1996**, *35*, 373.
(15) Kendelewicz, T.; Liu, P.; Doyle, C. S.; Brown, G. E. Spectroscopic study of the reaction of aqueous Cr(VI) with Fe3O4(111) surfaces. *Surf. Sci.* **2000**, *469*, 144−163.
(16) Poston, T. M.; Hanf, R. W.; Dirkes, R. L.; Morasch, L. F. "Hanford site environmental report for calendar year 2000," Pacific Northwest National Laboratory, 2001.
(17) Jones, T. E.; Watrous, R. A.; G. T., M. "Inventory estimates for single-shell tank leaks in S and SX tank farms," CH2M Hill Hanford Group, Inc., 2000.
(18) Zachara, J. M.; Ainsworth, C. C.; Brown, G. E.; Catalano, J. G.; McKinley, J., P.; Qafoku, O.; Smith, S. C.; Szecsody, J. E.; Traina, S. J.; Warner, J. A. Chromium speciation and mobility in a high level nuclear waste vadose zone plume. *Geochim. Cosmochim. Acta* **2004**, *68*, 13−30.
(19) Zachara, J. M.; Ainsworth, C. C.; Brown, G. E.; Catalano, J. G.; McKinley, J., P.; Qafoku, O.; Smith, S. C.; Szecsody, J. E.; Traina, S. J.; Warner, J. A. Chromium Speciation and Mobility in a High Level nuclear Waste Vadoes Zone Plume. *Geochim. Cosmochim.* **2004**, *68*, 13−30.
(20) Doyle, C. S.; Kendelewicz, T.; Brown, G. E. Inhibition of the reduction of Cr(VI) at the magnetite-water interface by calcium carbonate coatings. *Appl. Surf. Sci.* **2004**, *230*, 260−271.
(21) Peterson, M. L.; Brown, G. E.; Parks, G. A.; Stein, C. L. Differential redox and sorption of Cr(III/VI) on natural silicates and oxide minerals: EXAFS and XANES results. *Geochim. Cosmochim. Acta* **1997**, *61*, 3399−3412.
(22) Ilton, E. S.; Veblen, D. R. Chromium sorption by phlogopite and biotite in acidic solutions at 25 C: Insights from X-ray photoelectron and electron microscopy. *Geochim. Cosmochim. Acta* **1994**, *58*, 2777−2788.
(23) He, Y. T.; Traina, S. J. Cr(VI) reduction and immobilization by magnetite under alkaline pH conditions: The role of passivation. *Environ. Sci. Technol.* **2005**, *39*, 4499−4504.
(24) He, Y. T.; Chen, C. C.; Traina, S. J. Inhibited Cr(VI) reduction by aqueous Fe(II) under hyperalkaline conditions. *Environ. Sci. Technol.* **2004**, *38*, 5535−5539.
(25) Horton, D. G.; Schaef, H. T.; Serne, R. J.; Brown, C. F.; Valenta, M. M.; Vickerman, T. S.; Kutnyakov, I. V.; Baum, S. R.; Geiszler, K. N.; Parker, K. E. "Geochemistry of Samples from Borehole C3177 (299-E24-21)," Pacific Northwest National Laboratory, 2003.
(26) Walker, L. D. "Borehole summary report for the 2001 ILAW site characterization well," Bechtel Hanford, Inc., 2001.
(27) Stookey, L. L. A new spectrophotometric reagent for iron. *Anal. Chem.* **1970**, *42*, 779−781.
(28) Bartlett, R.; James, B. J. Behavior of chromium in soils: III. Oxidation. *J. Environ. Qual.* **1979**, *8*, 31−35.
(29) Webb, S. M. Sixpack: A graphical user interface for XAS analysis using IFEFFIT. *Phys. Scr.* **2005**, *T115*, 1011−1014.
(30) Newville, M. IFEFFIT: interactive XAFS analysis and FEFF fitting. *J. Synchrotron Radiat.* **2001**, *8*, 322−324.
(31) Ankudinov, A. L.; Rehr, J. J. Relativistic calculations of spin-dependent X-ray-absorption spectra. *Phys. Rev. B: Condens. Matter* **1997**, *15*, R1712−R1715.
(32) Newville, M.; Ravel, B.; Haskel, D.; Rehr, J. J.; Stern, E. A.; Yacoby, Y. Analysis of multiple-scattering XAFS data using theoretical standards. *Physica B* **1995**, *208 & 209*, 154−155.
(33) Hammersley, A. P. "FIT2D: An Introduction and Overview," European Synchrotron Radiation Facility, 1997.
(34) Hazemann, J. L.; Berar, J. F.; Manceau, A. Rietveld studies of the aluminum−iron substitution in synthetic goethite. *Phys. Chem. Miner.* **1991**, *19*, 25−38.
(35) Post, J. E.; Buchwald, V. F. Crystal structure refinement of akaganeite. *Am. Mineral.* **1991**, *76*, 272−277.
(36) Zachara, J. M.; Smith, S. C.; McKinley, J., P.; Serne, J. N.; Gassman, P. L. Sorption of Cs+ to micaceous subsurface sediments from the Hanford site. *Geochim. Cosmochim. Acta* **2002**, *66*, 193−211.
(37) White, G. N.; Dixon, J. B. In *Soil Mineraology with Environmental Applications*; Dixon, J. B., Schulze, D. G., Eds.; Soil Science Society of America: Madison, WI, 2002; Vol. 7, pp 389−414.
(38) Votyakov, S.; Chashchukhin, I.; Bykov, V.; Mironov, V. Behavior of Fe ions in minerals of ultrabasites during serpentinization. *Geochem. Int.* **1993**, *30*, 75−85.
(39) Fuchs, Y.; Linares, J.; Mellini, M. Mossbauer and infrared spectrometry of lizardite-1T from Monte Fico, Elba. *Phys. Chem. Miner.* **1998**, *26*, 111−115.

Received for review March 18, 2005. Revised manuscript received August 4, 2005. Accepted August 8, 2005.

ES050535Y